2020 IEEE International Conference on Systems, Man, and Cybernetics (SMC)
October 11-14, 2020. Toronto, Canada

Intrinsic Decomposition based Tensor Modeling Scheme for Hyperspectral Target Detection

Asma FEJJARI[1], Ouajdi KORBAA[3]
[1,3]MARS Research Laboratory, ISITCom, 4011, Hammam Sousse, University of Sousse, Tunisia.
[1]asmafejjari@gmail.com, [3]Ouajdi.Korbaa@centraliens-lille.org

Karim SAHEB ETTABAA[2]
[2]IMT Atlantique, Iti Department, Telecom Bretagne, 655 Street of Technopôle 29200 Plouzané, France.
[2]karim.sahebettabaa@riadi.rnu.tn

***Abstract*—Motivated by its capacity to process complex characteristics and deal with nonlinear problems, tensor decompositions have been also introduced, recently, to treat remote sensing data. In this article, a new tensor formulation based feature extraction framework is suggested for hyperspectral target detection. The new proposed method includes the intrinsic decomposition, as tensor structures, to improve the hyperspectral data representation and get rid of the non-significant spatial proprieties. Besides of the joint exploitation of spectral and spatial content, the new proposed approach allows to extract more effective discriminative spatial features. A series of experiments, for the purpose of hyperspectral target detection, show that the suggested scheme can be conducted on hyperspectral images with satisfactory detection accuracies.**

***Index Terms*— Tensor decompositions, feature extraction, target detection, intrinsic decomposition, hyperspectral images**.

I. INTRODUCTION

Hyperspectral image (HSI) is composed by several images taken on the same geographic area in the same time, according to many, narrow and adjoining spectral bands. Each image presents the way in which the Earth's surface reflects the sun incident light for a wavelength, and each pixel corresponds to a geographical position and a spectral luminance, which were observed in the near-infrared visible range (VNIR) [1]-[3]. The rich varieties of the HSI led to a wide range applicability in remote sensing fields such as medicine [4], agriculture [6] and microbiology [7]. Since this technology generates very high amounts of spectral redundancy, there is a need to lessen the spectral dimension without losing the interested information [8]. Besides spectral content, spatial details are paramount to enhance the accuracy. Hence, several extraction, classification and target detection methods that use spatial properties from HSI have been studied. The chief aim was to assign each image pixel to a class while taking into account both spectral and spatial data. Among these techniques, we can mention morphological decomposition [9], tensor presentation [10], segmentation algorithm [11] and Markov random field techniques [12].

Lately, tensor data modeling has attracted wide attention in the remote sensing field. Since HSI can be restructured as a three-order tensor: the first two dimensions correspond to the spatial positions while the third one to the spectral domain, the hyperspectral intrinsic data structure can be modeled using tensor based methods [3]. HSI tensor modeling was the fundamental focus of several research and has been used in a wide range of application such as anomaly and target detection [18]-[19], imagery classification and feature extraction [20]. Besides spectral components, tensor learning methods use spatial content, based on pixel spatial attributes extracted from the neighborhood, to present and process data. Spectro-spatial features exploitation permits to extract interested data with high efficiency and accuracy. Practically, non-relevant spatial features come off atmospheric variations, illuminations and sensor noise can affect hyperspectral scenes. As a result of such presence of datum within data processing and its negative impact on the accuracy, reducing non-relevant spatial information is a crucial step to ameliorate the tensor input feature representations. Various kinds of features can be employed to get rid of undesired spatial information and improve accuracy such as morphological features [9] and textures features [5]. In this manuscript, we used an intrinsic decomposition (ID) method based on energy optimization [15] to remove insignificant spatial data from hyperspectral scenes. The new proposed method preserves merely the reflectance properties and removes shape dependent proprieties.

By deploying the ID as tensor structures, we defined a tensor organization scheme to model the spectro-spatial properties of HSI data. The planned feature extraction method depends on three steps. Firstly, an ID process that aimed to remove the redundant and unimportant spatial information was employed. Secondly, a tensor based dimensionally reduction technique, called tensor principal component analysis (TPCA) [16], was used to lessen spectro-spatial tensor data redundancy. Lastly, we used the adaptive cosine/coherence estimator (ACE) detector [17] to detect targets. Comparing with the existing feature extraction approaches, the main contributions of this paper are:

- A new hyperspectral feature extraction scheme that uses the modeling of HSIs based on ID method as tensor structures was adopted for the first time.
- The proposed scheme deals with the use of spectro-spatial data, presented in HSIs, and their integration into the dimensionality reduction step.
- Remove useless and non-relevant spatial data, before the dimensionality reduction step, which performs better in data tensor organization and reduction.

978-1-7281-8526-2/20/$31.00 ©2020 IEEE

The rest parts of this paper are structured as follows: in section II, we made a description of our proposed approach. Afterwards, the experiments and the discussion are reported in section III. Finally, we conclude in section IV.

II. ID BASED TENSOR MODELING APPROACH

The current work aims to reach a more representative hyperspectral spectro-spatial feature structure. In this light, a supplemental ID was adopted, in this manuscript, to enhance the conventional tensor modeling scheme and obtain more compact hyperspectral feature representation. Thereupon, our suggested feature extraction approach includes three phases: in the first step, we apply an image ID based on energy minimization and weighting constraint. Secondly, a spectro-spatial dimension reduction process depended on the tensor PCA [16] method is performed to decrease redundant information. Ultimately, ACE [17] detector was opted to generate detection results. Our suggested approach is summarized in Fig.1.

A. ID process

The image ID [22] is a recent computer vision challenge that seeks to distinguish the different image physical components. In fact, the suggested methodology aims to differentiate the scene reflectance components from the shading ones (Fig.2). Recently, several strategies have been suggested to approximate reflectance and shading values [15], [23]. In this manuscript, we are particularly interested to the optimization decomposition method based on energy minimization [25]. An interesting aspect of the adopted method is its capacity to estimate the image intrinsic elements (reflectance, shading and illumination) with satisfactory rates. The employed approach looks to remove redundant and needless spatial data by getting rid of shadow dependent components (light and shape) and maintaining the scene reflectance properties (spectral properties). The ID (1) of an input photograph $\boldsymbol{I}$ generates two layers: reflectance components $\boldsymbol{R}$ and shading ones $\boldsymbol{S}$ [15].

$$\boldsymbol{I_i} = \boldsymbol{R_i}.\boldsymbol{S_i} \tag{1}$$

It is essential to note that $\boldsymbol{R_i}$ indicates the substance intrinsic color for an image pixel i. This metric is not liable to lighting and shading variations. $\boldsymbol{S_i}$ presents the reflected shading amount on an image pixel i. Accordingly, the scene ID depends on the estimation of the two elements $\boldsymbol{S_i}$ and $\boldsymbol{R_i}$ at each image pixel. By designating a local window, the image pixel values variations are often produced by the reflectance variations, which means that pixels those possess a similar intensities can generate similar reflectance values. Therefore, a pixel reflectance value can be computed as bellow:

$$\boldsymbol{R_i} = \sum_{j\in\varphi(i)} \vartheta_{ij}\boldsymbol{R_j} \tag{2}$$

While the term $\varphi(i)$ designates the local neighborhood window of the pixel i, ϑ_{ij} presents the reflectance resemblance between pixels i and j; it can be defined such that:

$$\vartheta_{ij} = e^{-(\boldsymbol{Y}_i-\boldsymbol{Y}_j)^2/(2\delta_i^2)} \tag{3}$$

We note that $\boldsymbol{Y}_i$ and $\boldsymbol{Y}_j$ describe respectively the intensity levels of pixels i and j, and δ_i is the intensity variance presented in the local neighborhood window. In this light, the weight expression can be enhanced as bellow:

$$\vartheta_{ij} = e^{[(\boldsymbol{Y}_i-\boldsymbol{Y}_j)^2/(\delta_{iY}^2)+H(\boldsymbol{I}_i,\boldsymbol{I}_j)^2/(\delta_{iH}^2)]} \tag{4}$$

$H(\boldsymbol{I}_i,\boldsymbol{I}_j)$ denotes the angle between the two vectors $\boldsymbol{I}_i$and $\boldsymbol{I}_j$, δ_{iH} and δ_{iY} correspond to angle variance and pixel values in the local neighborhood window around the pixel i. Since variations in shading values depend on proportional color channel value changes, the shading component $\boldsymbol{S}$ could be eliminated from the original scene. Optimize the energy function $\boldsymbol{E}$ $\boldsymbol{(R, S)}$ presents an effective way to produce the reflectance $\boldsymbol{R}$ element:

$$\operatorname{argmin}_{\boldsymbol{R},\boldsymbol{S}} \boldsymbol{E}\,(\mathbf{R}, \boldsymbol{S}) = \sum_{i\in I}(\boldsymbol{R}_i - \sum_{j\in\varphi(i)} \vartheta_{ij}\boldsymbol{R}_i)^2 - \sum_{i\in I}(\boldsymbol{I}_i/\boldsymbol{S}_i - \boldsymbol{R}_i)^2 \tag{5}$$

B. Tensor decomposition and dimension reduction process

Since it can keep the initial data rearrangement and preserve spectro-spatial pixel relationships, tensor decomposition based methods have become standard tools for feature extraction, dimensional reduction and classification tasks. In this section, we introduce how to exploit tensor decomposition bases to handle the data obtained with the ID methodology. According to the multilinear algebra theory [13], a tensor $\boldsymbol{A} \in \mathbb{R}^{L_1\times L_2\times\ldots\times L_N}$, where N presents the tensor order, can be considered as a higher rank form of a vector and matrix structure. Mathematically, a tensor can be defined as a multidimensional array of components. Such element of $\boldsymbol{A}$ is a scalar $a_{l_1,l_2,\ldots,l_N}$; where l_i presents the element's position in the i^{th} mode. We note that $1\leq l_i \leq L_i$ and $1\leq i \leq N$. Since HSI is by nature a three dimensional block of data, hyperspectral databases can be modeled using 3-order tensor $\boldsymbol{A} \in \mathbb{R}^{L_1\times L_2\times L_3}$. The two first orders correspond to pixel spatial locations while the third mode presents spectral domain.

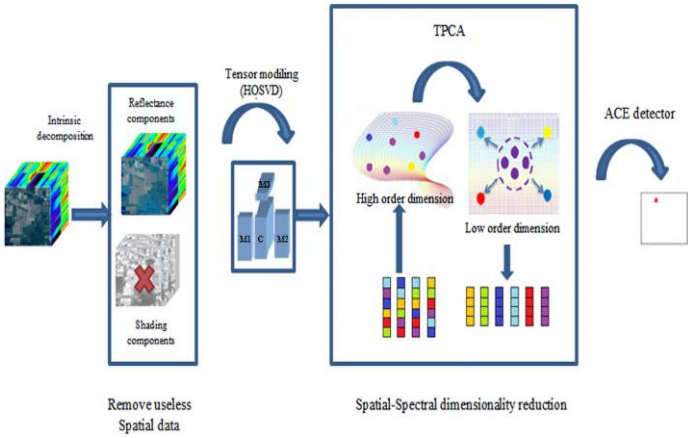

Fig. 1. Flowchart of the new proposed approach.

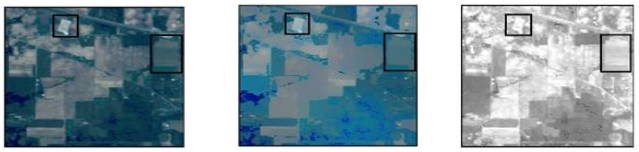

(a) (b) (c)

Fig. 2. Illustration of image ID: (a) Input image, (b) reflectance components, and (c) shading components.

In the last few years, many tensor decomposition based approaches have been proposed. These approaches include Canonical Polyadic decomposition (CP) and Tucker decomposition (TKD) [24]. In this paper, the high order singular value decomposition (HOSVD) [26] method was adapted to model HSI data as tensor. The goal of the HOSVD method is to decompose an *N*-order tensor $\boldsymbol{R} \in \mathrm{R}^{I_1 \times I_2 \times I_3 \times \ldots \times I_N}$ into a core tensor $\boldsymbol{C}$ and a series of factor matrices $\boldsymbol{M}_n$. This can be explained as follows: the core tensor $\boldsymbol{C}$ defines the relation between factor matrices $\boldsymbol{M}_n$ while $\boldsymbol{M}_n$ include the orthonormal vectors consisting of the column space of the matrix $\boldsymbol{R}_n$, generated from the mode-*n* flattening of $\boldsymbol{R}$. The Alternative Least Square (ALS) [14] algorithm, performed by the HOSVD method, was implemented to produce mode-*n* matrices $\boldsymbol{M}_n$ [13]. Accordingly, the reflectance component can be defined such that:

$$\boldsymbol{R} = \boldsymbol{C} \times_1 \boldsymbol{M_1} \times_2 \boldsymbol{M_2} \times_3 \ldots \times_N \boldsymbol{M_N} \quad (6)$$

In the case of HSI, HOSVD method tends to determine the core tensor $\boldsymbol{C}$ and the basic matrices $\boldsymbol{M}_1$, $\boldsymbol{M}_2$ and $\boldsymbol{M}_3$ by minimising the L_2-norm reconstruction error:

$$min_{\boldsymbol{M_1},\boldsymbol{M_2},\boldsymbol{M_3},\boldsymbol{C}} \boldsymbol{E_{r1}} = || \boldsymbol{R} - \boldsymbol{C} \times_1 \boldsymbol{M_1} \times_2 \boldsymbol{M_2} \times_3 \boldsymbol{M_3} ||^2 \quad (7)$$

According to the orthogonality assumption, we can write:

$$\boldsymbol{B} = \boldsymbol{R} \times_1 \boldsymbol{M}_1^T \times_2 \boldsymbol{M}_2^T \times_3 \boldsymbol{M}_3^T \quad (8)$$

Hence (7) can be reformulated as below:

$$min_{\boldsymbol{M_1},\boldsymbol{M_2},\boldsymbol{M_3}} E_{r1} = ||\boldsymbol{R}||^2 - ||\mathbf{B}||^2 \quad (9)$$

$$= max_{\boldsymbol{M_1},\boldsymbol{M_2},\boldsymbol{M_3}} E_{r2} = ||\mathbf{B}||_F^2 \quad (10)$$

In this case, the statement (10) is identical to maximize:

$$\begin{aligned} \max_{\boldsymbol{M_1},\boldsymbol{M_2},\boldsymbol{M_3}} E_{r2} &= \text{Trace}\,(\boldsymbol{M}_1^T \boldsymbol{Q}\, \boldsymbol{M}_1) \\ &= \text{Trace}\,(\boldsymbol{M}_2^T\, \boldsymbol{U}\, \boldsymbol{M}_2) \\ &= \text{Trace}\,(\boldsymbol{M}_3^T\, \boldsymbol{P}\, \boldsymbol{M}_3) \end{aligned} \quad (11)$$

$\boldsymbol{Q}$, $\boldsymbol{U}$ and $\boldsymbol{P}$ are semipositive definite matrices and they were implemented as mentioned in [9], [21].

Because of the enormous dimensions of HSI data, the proposed scheme would be computationally very heavy. One solution to lessen the computational burden and avoid problems generated when working in huge dimensional feature subspaces is to pass by a pre-processing stage. This can be done by reducing the tensor data dimensions without losing significant information. In this manuscript, the TPCA [16] method was performed to lower the resulting tensor dimensions. TPCA is the tensorial variant of the PCA [27] approach where the input data are formulated as higher order tensors. To retain the major part of the initial tensorial input variation, the suggested feature extraction scheme adopts multilinear projection concept. For hyperspectral data, the TPCA [9] estimation of an image $\boldsymbol{R}$ of dimensions n_1 ,n_2, n_3 is determined as follows:

$$\widehat{\boldsymbol{R}} = \boldsymbol{R} \times_1 \widehat{\boldsymbol{M}_{J_1}} \widehat{\boldsymbol{M}}_{J_1}^T \times_2 \widehat{\boldsymbol{M}_{J_2}} \widehat{\boldsymbol{M}}_{J_2}^T \times_3 \widehat{\boldsymbol{M}}_k^T \quad (12)$$

We note that $\widehat{\boldsymbol{M}_{J_1}}$ and $\widehat{\boldsymbol{M}_{J_2}}$ possess the J_1 and J_2 largest eigenvectors related to the unfolding matrix $\boldsymbol{R}_1$ and $\boldsymbol{R}_2$ respectively. $\widehat{\boldsymbol{M}}_k^T$ contains the *k*-largest eigenvectors related to the unfolding matrix $\boldsymbol{R}_3$. If we consider that $J_1 = n_1$, $J_2 = n_2$, $\widehat{\boldsymbol{M}_{J_1}} \widehat{\boldsymbol{M}}_{J_1}^T = \boldsymbol{I}_{n_1 \times n_1}$ and $\widehat{\boldsymbol{M}_{J_2}} \widehat{\boldsymbol{M}}_{J_2}^T = \boldsymbol{I}_{n_2 \times n_2}$, the formula (12) can be reformulated as bellow:

$$\widehat{\boldsymbol{R}} = \boldsymbol{R} \times_3 \widehat{\boldsymbol{M}}_k^T \quad (13)$$

III. Experimental Analysis and Results

A. Data sets and parameter analysis

The suggested approach was evaluated on three real hyperspectral scenes selected from Airport-Beach-Urban (ABU) hyperspectral database and collected from AVIRIS (Airborne Visible/Infrared Imaging Spectrometer) sensor system. The three tested scenes include:

a. Airport-2: The first tested scene was captured in Los angles in November, 2011. It contains 205 bands of size 100 × 100 pixels and a spatial resolution of 7,1 m/pixel.

b. Beach-2: The second proposed image includes 193 bands taken in San Diego, in November of 2011. Each spectral band has 100 × 100 pixels. The HSI has a spatial resolution of 7,5 m/pixel.

c. Urban-2: The last used hyperspectral scene, of size 100 × 100 pixels, was picked up in August, 2010 in Texas Cost. The urban-2 image has 207 spectral bands and a spatial resolution of 17,2 m/pixel.

All the tested images and their reference maps were downloaded from [28]. Fig. 9 (First and second column) shows the used hyperspectral scenes and their reference detection maps. Four feature extraction techniques were used to assess the proposed methodology during the target detection tasks: 3D Wavelet filter [29], 3D Gabor filter [30], morphological decomposition (MD) method [9] and TPCA approach [16]. The ACE detector [17] was deployed in the detection process to compare the qualitative results. The receiver operating characteristic (ROC) curve and the area under the curve (AUC) were performed for target detection evaluation [31]. The ROC curve is computed from true positive rate (*TPR*) versus false positive rate (*FPR*) at different values of threshold. *TPR* and *FPR* values, computed from four parameters: True positive (*TP*), false positive (*FP*), true negative (*TN*) and false negative (*FN*) pixels at a series of threshold, can be established as follows:

$$TPR = TP/\,(TP + FN) \quad (14)$$

$$FPR = FP/\,(FP + TN) \quad (15)$$

The area under the curve (*AUC*) metric is also depending on *TPR* and *FPR*.

$$AUC = \int_{-\infty}^{+\infty} TPR(T) FPR'(T) dT \quad (16)$$

T is the chosen threshold; it was fixed from 0 to 255 during the detection process. Achieving a high AUC score allows to get a low false alarm and a high value of target pixels.

The choice of optimal parameters employed during the target detection process will be analyzed with details in this section. Three parameters should be set: the local window radius ($\boldsymbol{\varphi}$) for the ID process, the parameters J_1 and J_2 employed for

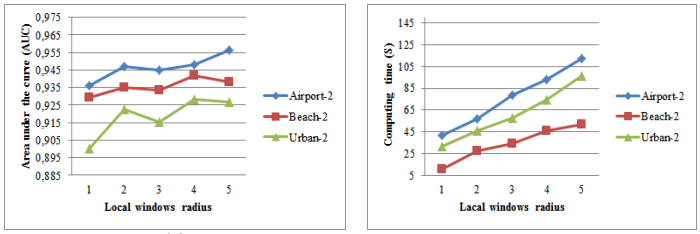

(a) (b)

Fig. 3. Detection rate of image ID with different various of **φ**: (a) AUC scores and (b) execution time.

spatial dimension reduction, and the reduced bands number.

a. Local window radius φ: at first time, we will estimate the optimal value of φ applied throughout the ID phase. We judged the target detection rate employing AUC scores and running time requirements. Fig. 3 (a) shows the AUC rate, according to the radius φ. Through this figure, the best AUC scores were achieved when φ is set at 4. This radius gave an AUC by about 0.9481, 0.9417 and 0.9289 for the Airport-2, Beach-2 and Urban-2 scenes respectively, and it needed about 93s to process the first scene, 46s for the second and 75s for the third one. Select φ = 4 pixels is relatively expensive aside computing time. Owing to its ability to offer a satisfied AUC score with a low computing time, we adopted φ = 2 for the entire tested scenes.

b. Parameters J_1 and J_2 : as mentioned previously, these parameters are used during spatial dimension reduction. The parameters $J_1$and J_2 were picked in accordance with AUC scores and computing time. AUC scores, for each image, are illustrated in Fig. 4 (a), (c) and (e), the best scores can be achieved with J_1 = 5 and of J_2 = 10 for Airport-2 and Urban-2 scenes, these last gave an AUC = 0.9657 for the first image and AUC = 0.9636 for the second one. For the Beach-2 image, J_1 = 10 and J_2 = 10 allow to get the best AUC score (0.973). It is also shown that the execution time of the new proposed approach elevates when the selected eigenvectors number is rising. Thence, using a little number of J_1 and J_2 corresponds to a tradeoff between detection aptitude and computing performance.

c. Spectral reduced dimensionality for TPCA: this parameter is selected according to the performance of AUC. Fig. 5 shows the AUC scores and the execution time obtained by different number of features. It can be noticed that our proposed method can obtain the highest AUC score, i.e., AUC = 0.982 for Airport-2 and AUC = 0.985 for Beach-2 when the number of selected features is near 25 and AUC = 0.9796 for Urban-2 when the reduced features is equal to 15. As the running time of the new proposed method increases in accordance with features number, 25 is selected to be the optimal reduced dimension for Airport-2 and Beach-2 scenes, whereas 15 is selected for the Urban-2 data set.

B. Results

This part is dedicated to assess the proposed scheme performance during the detection tasks. Detection results were judged using AUC scores, ROC curves, execution time and detection maps.

a. Airport-2: ROC curves and AUC scores for all tested techniques are presented in Fig. 6 (a)-(b). According to the ROC curves, our suggested method has always exhibited a higher true positive rate when the false positive rate varies from 0 to 1. Moreover, it can be seen that the suggested approach paves the way for a better result than all other tested

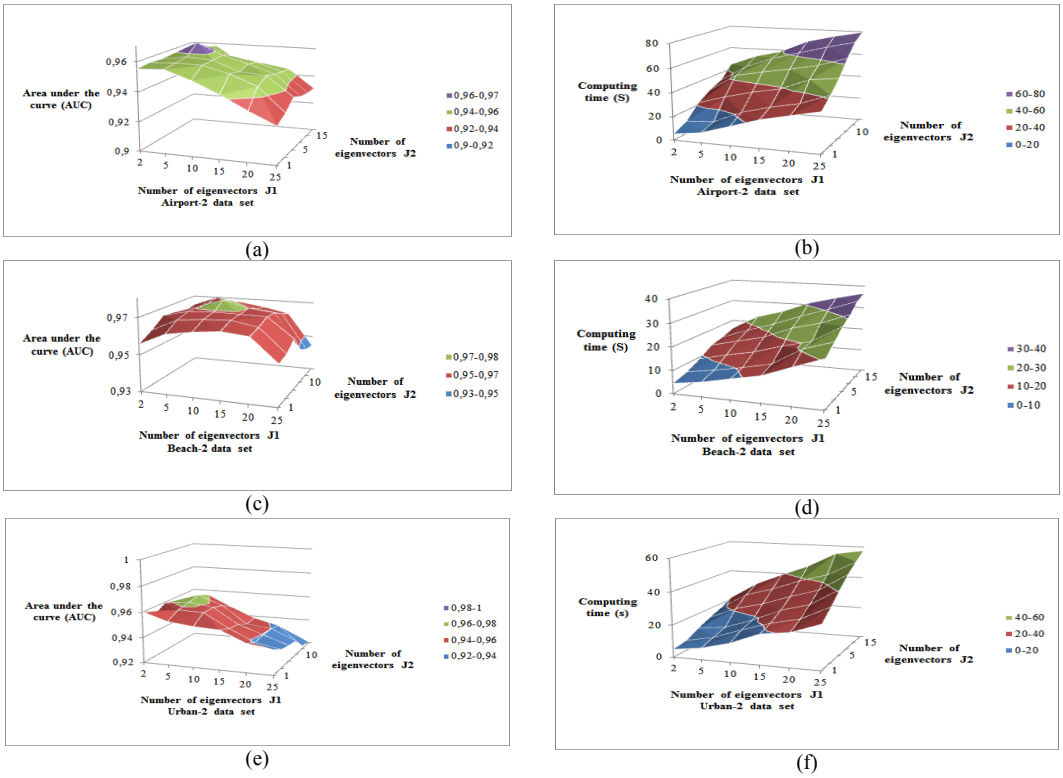

(a) (b) (c) (d) (e) (f)

Fig. 4. AUC scores and running time, respect to J_1 and J_2 of (a) and (b) Airport-2, (c) and (d) Beach-2 and (e) and (f) Urban-2.

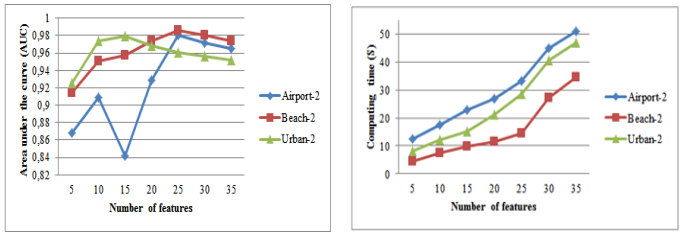

(a) (b)

Fig. 5. The reduced dimensionality in TPCA: (a) AUC scores and (b) computing time.

methods since its confidence bounds are always higher than others, when TPR varies from 0 to 1. In addition, the new proposed method achieved the highest AUC scores; it gave the highest one by about 0.98 followed by 3D Gabor filter (0.936) then 3D Wavelet filter (0.895). The detection maps of all compared methods are displayed in Fig. 9 (first row). By studying these maps, we find that our proposed approach tends to be less attracted by false detection. It can detect the airplanes clearly. Furthermore, the shapes of the objects of interest are also very clear in our detection results. TPCA and morphological decomposition methods perform badly in the airport scene. Even though they can detect the positions of the two airplanes, some details of the airplane are still missing. For instance, 3D wavelet filter is the most attracted by false detection alarms.

b. Beach-2: Fig. 7 (a)-(b) shows the ROC curves and the AUC scores of Beach-2 image. According to this figure, the best ROC curves and AUC scores were fulfilled by our proposed approach, i.e. the new approach has been able to extract useful information of interest objects with a low rate of false alarm. The worst detection results were obtained from TPCA and morphological decomposition. The 3D filter Gabor (AUC = 0.9491) exhibited a near performance of the new proposed approach (AUC = 0.9851). Fig. 9 (second row) presents the detection maps of the second detested scene. By visualizing the detection maps, we find that our proposed approach can better highlight the interest objects, in spite of different sizes and areas. For example, the target objects in the ocean area can be well detected than 3D Gabor and 3D wavelet filters. TPCA and morphological methods usually have the least detection performances: AUC = 0.5323 and 0.7621 for the Tensor PCA and morphological methods, respectively.

c. Urban-2: The assessment of different tested approaches according to ROC, AUC index and computing time appears in Fig. 8 (a)-(c). As noticed in the two first tested images (Airport-2 and Beach-2), the new proposed approach provides the best detection rates (AUC = 0.9756) with the least false alarms (about 0.1) and the highest computing time. Fig. 9 (third row) displays the detection maps for the third evaluated

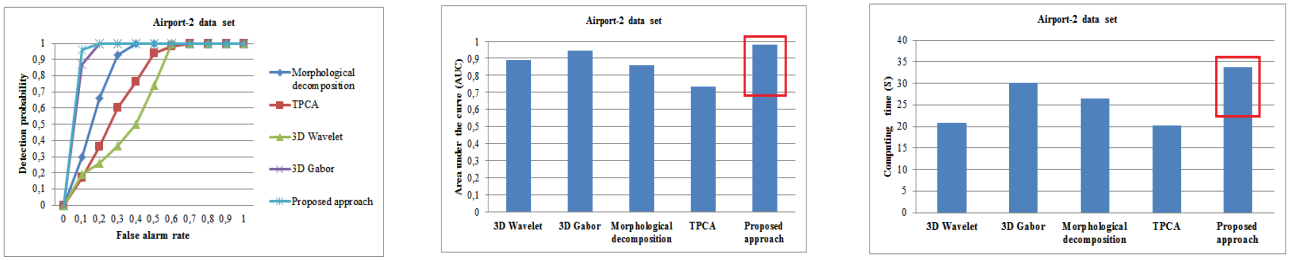

(a) (b) (c)

Fig. 6. Detection results for Airport-2 data set: (a) ROC curves, (b) AUC scores and (c) computing time.

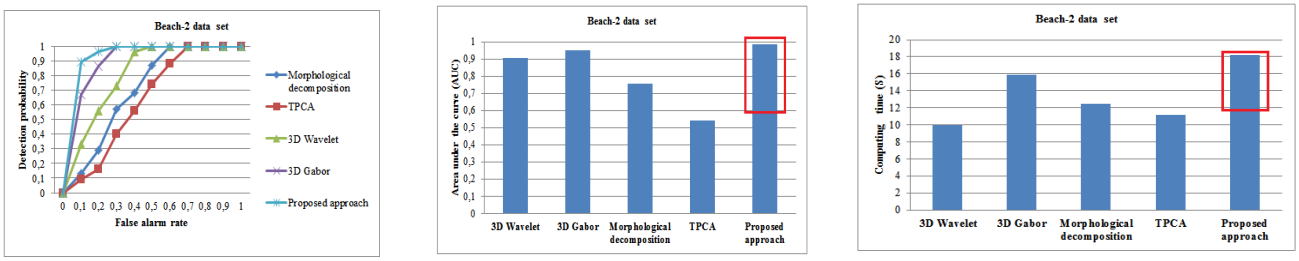

(a) (b) (c)

Fig. 7. Detection results for Beach-2 data set: (a) ROC curves, (b) AUC scores and (c) computing time.

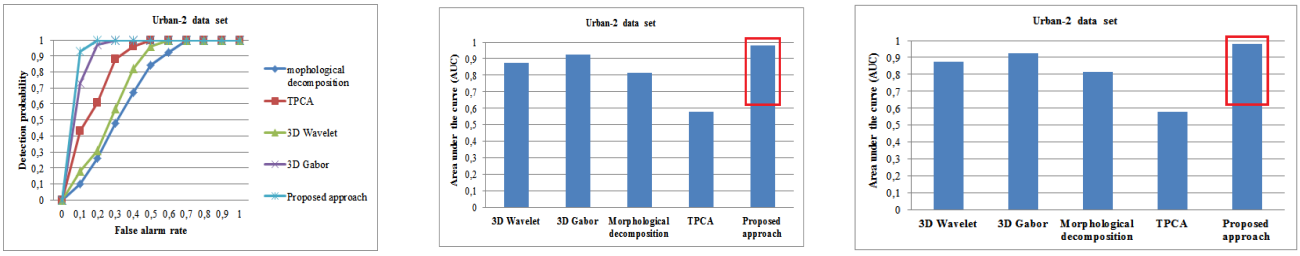

(a) (b) (c)

Fig. 8. Detection results for Urban-2 data set: (a) ROC curves, (b) AUC scores and (c) computing time.

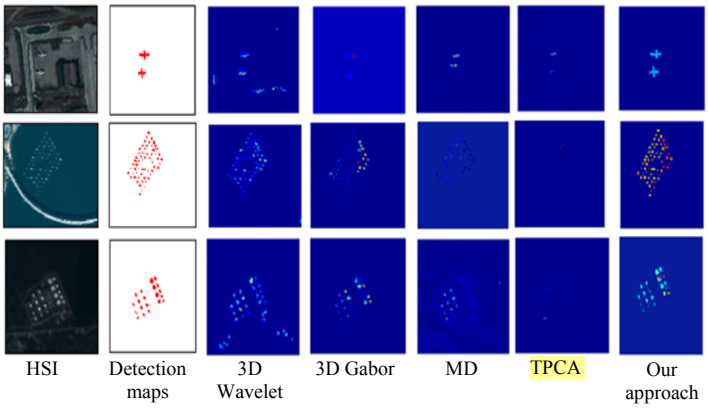

Fig. 9. Detection maps of the Airport-2 (first row), Beach-2 (second row) and Urban-2 (third row) images with all tested approaches.

data set. The urban area is well detected with the new proposed approach and 3D Gabor filter technique, while the wavelet and morphological contained false alarms.

IV. Conclusion

The new proposed approach deals with the joint employ of spectral and spatial data procured by the hyperspectral scenes. An ID process based on energy optimization is firstly proposed. The ID method is used to exclude useless and insignificant spatial data from the hyperspectral scene without any loss of information. The resulted data is reformulated as a tensor structure, and the tensor principal component analysis (TPCA) approach is used then to reduce the spectro-spatial dimension. Compared with the standard tensor modeling approach, the novel proposed method incorporates more significant spatial information during dimensionality reduction. Although experiments, on several real hyperspectral scenes, have demonstrated that our proposed approach can significantly enhance the target detection rates, the proposed technique suffers from high computing time compared to the other tested approaches.

ACKNOWLEDGMENT

This work was supported and financed by the Ministry of Higher Education and Scientific Research of Tunisia.

REFERENCES

[1] J. Ren, R. Wang, G. Liu, R. Feng, Y. Wang, and W. Wu, "Partitioned Relief-F Method for Dimensionality Reduction of Hyperspectral Images," Remote Sensing, vol. 12, no. 7, March 2020.

[2] A. Fejjari, K. Saheb Ettabaa, and O. Korbaa, "Modified Graph-Based Algorithm for Efficient Hyperspectral Feature Extraction," International Symposium on Computer and Information Sciences ISCIS 2018: Computer and Information Sciences, pp. 87-95.

[3] L. Zhang, L. Zhang, D. Tao, and X. Huang, "Tensor Discriminative Locality Alignment for Hyperspectral Image Spectral–Spatial Feature Extraction," IEEE Transactions on Geoscience and Remote Sensing, vol. 51, no. 1, pp. 242-256, January 2013.

[4] G. Lu, L. Halig, D. Wang, Z.G. Chen, and B. Fei, "Spectral-Spatial Classification using Tensor Modeling for Cancer Detection with Hyperspectral Imaging," SPIE, March 2014.

[5] C. Xie and Y. He, "Spectrum and Image Texture Features Analysis for Early Blight Disease Detection on Eggplant Leaves," Sensors, vol. 16, no. 6, May 2016.

[6] N. Zaini, F. van der Meer, and H. van der Werff, "Determination of Carbonate Rock Chemistry using Laboratory-Based Hyperspectral Imagery," Remote Sensing , vol. 6, no. 5, pp. 4149-4172, May 2014.

[7] A.A. Gowen, Y. Feng, E. Gaston, and V. Valdramidis, "Recent applications of hyperspectral imaging in microbiology," Talanta, vol. 137, pp. 43-54, May 2015.

[8] A. Fejjari, K. Saheb Ettabaa, and O. Korbaa, "Fast spatial spectral Schroedinger Eigenmaps algorithm for hyperspectral feature extraction". Procedia Comput. Sci. vol. 126, pp. 656–664, September 2018.

[9] S. V. Forero and J. Angulo, "Classification of hyperspectral images by tensor modeling and additive morphological decomposition," Pattern Recognition, vol. 46, no. 2, pp. 566-577, August 2012.

[10] H. Wang and N. Ahuja, "A Tensor Approximation Approach to Dimensionality Reduction," Int. J. Comput. Vis., vol. 76, pp. 217–229, March 2008.

[11] J. Li, J.M. Bioucas-Dias, and A. Plaza, "Hyperspectral Image Segmentation using a New Bayesian Approach with Active Learning," IEEE Transactions on Geoscience and Remote Sensing, vol. 49, no. 10, pp. 3947-3960, November 2011.

[12] J. Li, J. M. Bioucas-Dias, and A. Plaza, "Spectral–Spatial Hyperspectral Image Segmentation Using Subspace Multinomial Logistic Regression and Markov Random Fields," IEEE Transactions on Geoscience and Remote Sensing, vol. 50, no. 3, pp. 809–823, March 2012.

[13] H. Lu, K. N. Plataniotis, and A. N. Venetsanopoulos, "A survey of multilinear subspace learning for tensor data," Journal Pattern Recognition, vol. 44, no. 7, pp. 1540-1551, July 2011.

[14] P. Comon, X. Luciani, and A. L. F. De Almeida, "Tensor Decompositions, Alternating Least Squares and other Tales," Journal of Chemometrics, vol. 23, pp. 393–405, August 2009.

[15] J. Shen, X. Yang, Y. Jia, and X. Li, "Intrinsic images using optimization," The 24th IEEE Conference on Computer Vision and Pattern Recognition CVPR, pp. 3481–3487, 2011.

[16] Y. Ren, L. Liao, S. J. Maybank, Y. Zhang, and X. Liu, "Hyperspectral Image Spectral-Spatial Feature Extraction via Tensor Principal Component Analysis," IEEE Geoscience and Remote Sensing Letters, vol. 14, no. 9, pp. 1431-1435, September 2017.

[17] B. Alvey, A. Zare, M. Cook, and D. K. Ho, "Adaptive coherence estimator (ACE) for explosive hazard detection using wide band electromagnetic induction (WEMI)," SPIE, vol. 982309-7, May 2016.

[18] J. Tan, J. Zhang, and Y. Zhang, "Target Detection for Polarized Hyperspectral Images Based on Tensor Decomposition," IEEE Geoscience and Remote Sensing Letters, vol. 14, no. 99, pp. 674–678, March 2017.

[19] Y. Liu, G. Gao, and Y. Gu, "Tensor Matched Subspace Detector for Hyperspectral Target Detection," IEEE Transactions on Geoscience and Remote Sensing , vol. 55, no. 4, pp. 1967–1974, April 2017.

[20] Z. Zhong, B. Fan, J. Duan, L. Wang, K. Ding, S. Xiang, and C. Pan, "Discriminant Tensor Spectral–Spatial Feature Extraction for Hyperspectral Image Classification," IEEE Geoscience and Remote Sensing Letters, vol. 12, no. 5, pp. 1028-1032, May 2015.

[21] S. Velasco-Forero and J. Angulo, "Parameters selection of morphological scale-space decomposition for hyperspectral images using tensor modeling," SPIE, vol. 7695, pp. 1–12, 2010.

[22] H. G. Barrow and J. M. Tenenbaum, "Recovering Intrinsic Scene Characteristics from Images," In Computer Vision Systems, Eds. 1978, New York: Academic, pp. 3–26.

[23] E. H. Land and J. J. McCann, "Lightness and retinex theory," Journal of the Optical Society of America, vol. 61, no. 1, pp. 1–11, January 1971.

[24] A. Cichocki, D. Mandic, L. De Lathauwer, G. Zhou, Q. Zhao, C. Caiafa, and H. Phan, "Tensor Decompositions for Signal Processing Applications: From two-way to multiway component analysis". IEEE Signal Process. Mag. vol. 32, pp. 145–163, March 2015.

[25] J. Shen, X. Yang, X. Li, and Y. Jia, "Intrinsic Image Decomposition using Optimization and User Scribbles," IEEE Transactions on Cybernetics, vol. 43, no. 2, pp. 425-36, April 2013.

[26] G. Bergqvist and E. G. Larsson, "The Higher-Order Singular Value Decomposition: Theory and an Application [Lecture Notes]," IEEE Signal Processing Magazine, vol. 27, no. 3, pp. 151-154, May 2010.

[27] A. Fejjari, K. Saheb Ettabaa, and O. Korbaa, "Feature Extraction Techniques for Hyperspectral Images Classification," International Workshop Soft Computing Applications SOFA 2018: Soft Computing Applications, pp. 174-188.

[28] Xudong Kang's home page, [Online]. Available: http://xudongkang.weebly.com/data-sets.html, accessed on: 11 October 2019.

[29] B. Rasti, J. R. Sveinsson, M.O. Ulfarsson, and J. A. Benediktsson, "Hyperspectral Image Denoising Using 3d Wavelets," IEEE International Geoscience and Remote Sensing Symposium (IGARSS), pp. 1349-1352, July 2012.

[30] T. C. Bau and G. Healey, "Rotation and Scale Invariant Hyperspectral Classification Using 3D Gabor Filters," SPIE, vol. 7334, 2009.

[31] P. Flach, J. Hernández-Orallo, and C. Ferri, "A coherent interpretation of AUC as a measure of aggregated classification performance," The 28th International Conference on Machine Learning, pp. 657–664, 2011.